Comparison of $CaMn_{1-x}Ru_xO_3$ and $CaMn_{1-y}Mo_yO_3$ perovskites

L. Pi, S. Hébert, C. Martin, A. Maignan,* and B. Raveau

Laboratoire CRISMAT, UMR 6508 associée au CNRS, ISMRA et Université de Caen, 6 Boulevard du Maréchal Juin, 14050 Caen Cedex, France

(Received 2 August 2002; published 30 January 2003)

The structure, resistivity, thermopower, and magnetic behaviors of two sets of samples $CaMn_{1-x}Ru_xO_3$ and $CaMn_{1-y}Mo_yO_3$ ($0.04 \leq x \leq 0.08$; $0.02 \leq y \leq 0.04$) have been studied. All samples exhibit a magnetoresistance effect. The high-temperature region of all samples can be fitted well by a small polaron hopping model. The activation energy of Ru-doped samples decreases with doping while that of Mo-doped samples increases. However, for the same Mn valency, the Mo-doped system exhibits ferromagnetism in contrast to the Ru-doped $CaMnO_3$. The antiferromagnetic state of $CaMn_{0.94}Ru_{0.06}O_3$ has been confirmed by neutron diffraction. This strongly suggests that the Ru^{5+}-O-Mn^{4+} antiferromagnetic superexchange for low doping levels prevails over ferromagnetic exchanges, i.e., Mn^{3+}-O-Mn^{4+} and Ru^{5+}-O-Mn^{3+} interactions. These electron-doped oxides exhibit large absolute values of thermopower at room temperature (Seebeck coefficient $|S| > 100 \, \mu V \, K^{-1}$) accompanied by low values of their resistivity ($\rho < 0.03 \, \Omega$ cm) and thermal conductivity ($\kappa \sim 5 \, W \, K^{-1} \, m^{-1}$). Therefore, they are good candidates for applications as n-type legs of thermopower generators to be used at high temperatures ($T \gg 300$ K).

INTRODUCTION

Manganites with perovskite structure have been widely investigated after colossal magnetoresistance (CMR) was found in $La_{1-x}Ba_xMnO_3$ by Helmolt *et al.*[1] in 1993. The basic mechanism for transport in these oxides is believed to be double-exchange (DE) together with the Jahn-Teller (JT) effect.[2,3] Most of the studies concentrated on the hole-doped manganites $L_{1-x}A_xMnO_3$ ($x < 0.5$),[4–8] where L is a lanthanide and A is an alkaline-earth cation, while the electron-doped manganites such as $L_{0.25}Ca_{0.75}MnO_3$ which correspond to Mn^{4+}-rich contents, have not been extensively studied since they do not exhibit magnetoresistance effects.[9–11] In recent years, the discovery of new ferromagnetic (FM) metallic manganites $Ca_{1-x}L_xMnO_3$ and $Ca_{1-x}Bi_xMnO_3$ ($x \sim 0.10$) (Refs. 12 and 13) has attracted much attention because it suggests the possibility of magnetoresistance effects for electron-doped systems. The latter investigation of the series $L_{1-x}Ca_xMnO_3$ in the range $0.80 \leq x \leq 1$ demonstrated this.[14]

We know that these A-site-doped oxides $L_{1-x}A_xMnO_3$ with high Mn^{4+} content have a large absolute value of thermopower (S) at room temperature.[15] Since their S value is increasingly negative with increasing temperature, these oxides are interesting as n-type legs for a thermoelectric device in air at high temperature.[16] It has also been shown that substituting the Mn site of $CaMnO_3$ with a high-valency metal (superior to +4) can induce Mn^{3+} species and consequently lead to CMR.[17–21] So it is interesting to check if Mn-site-doped manganites would also have large absolute S values in the low doping range. In this paper, we compare the structure, resistivity, magnetism, and thermopower results between lightly doped $CaMn_{1-x}Ru_xO_3$ and $CaMn_{1-y}Mo_yO_3$, which are promising thermoelectric materials. It is shown that these magnetic and nonmagnetic substituted cations induce different properties in the low-doping regime.

EXPERIMENT

$CaMn_{1-x}Ru_xO_3$ and $CaMn_{1-y}Mo_yO_3$ ceramic samples were synthesized in the form of bars at 1400 °C in air according to the procedure detailed in Refs. 17 and 18. X-ray patterns were registered at room temperature (RT) by using a Philips diffractometer working with Cu $K\alpha$ radiation. Neutron powder diffraction data were also obtained, versus temperature, for the $CaMn_{0.94}Ru_{0.06}O_3$ composition, in Laboratoire Léon Brillouin Saclay (France). The patterns were recorded on the G41 diffractometer ($\lambda = 2.4266$ Å) from 1.4 to 300 K by steps of 5 K. All these data were refined by using the FULLPROF program.

The magnetization M data were recorded upon warming with a dc superconducting quantum interference device (SQUID) magnetometer (0–5 T, 5–400 K). The resistivity of the samples was measured using standard four-probe method in a Physical Properties Measurements System Quantum Design system (5–300 K, 0–7 T). The thermoelectric power (TEP) and thermal conductivity measurements were carried out in the same PPMS Quantum Design system. The four-point steady-state method with separated measuring and power contacts (sample extremities) was applied to eliminate the thermal resistances between the sink and the heater, respectively. The temperature gradient and voltage drop were monitored using two separated differential chromel-constantan thermocouples. A typical temperature difference across the sample was 1.5 K. The influences of the thermopower of chromel, in the case of thermovoltage measurements, sample radiation, and thermal conductivity of differential thermocouples, in the case of thermal conductivity measurements, were carefully taken into account and corresponding corrections were made. The experimental setup was checked using reference samples and the error within all range of temperatures did not exceed absolutely $\sim 1 \, \mu V \, K^{-1}$ (thermopower) and $\sim 0.1 \, W \, m^{-1} \, K^{-1}$ (thermal conductivity) or relatively of 5% of measured value.
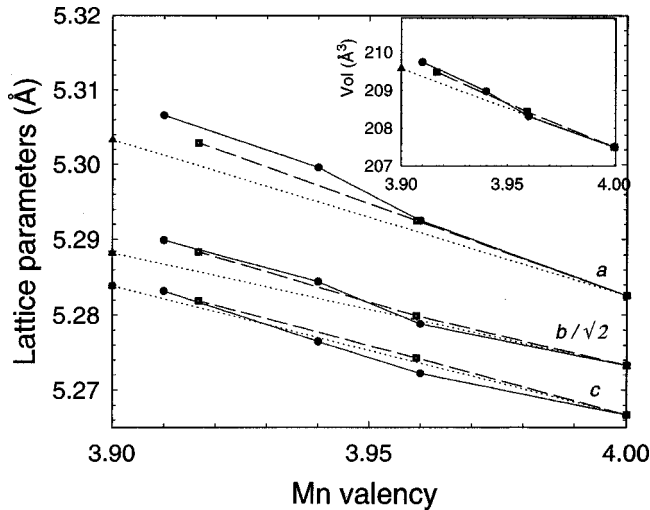
FIG. 1. Mn valency dependence of the RT lattice parameters (and volume in inset) for the $CaMn_{1-x}Ru_xO_3$ (circles), $CaMn_{1-y}Mo_yO_3$ (squares) and $Sm_{1-x}Ca_xMnO_3$ (triangles) series. The lines are only a guide for the eye.

RESULTS AND DISCUSSION

Valency of ruthenium in $CaMn_{1-x}Ru_xO_3$

In our previous studies, the results of the substitution at the Mn site has been investigated on the basis of a "valency" effect. Substituting an M cation characterized by a larger oxidation state than tetravalent in $CaMnO_3$ creates Mn^{3+} species that are able to participate in a Mn^{3+}-O-Mn^{4+} double exchange responsible for the resistivity decrease, weak ferromagnetism, and CMR properties. Nevertheless, for M = Ru the situation is not so simple if one takes into account the possible Ru^{4+}/Ru^{5+} oxidation states encountered for ruthenium in oxides. In order to clarify this point, the RT structural parameters of several $CaMn_{1-x}Ru_xO_3$, $CaMn_{1-y}Mo_yO_3$, and $Sm_{1-x}Ca_xMnO_3$ (Ref. 21) series have been refined in the *Pnma* space group and compared. It should be pointed out that the cell parameters and unit-cell volume of these manganites are very sensitive to the Mn valency. This is explained by the large difference of ionic radius between Mn^{3+} and Mn^{4+}. By supposing pentavalent ruthenium, one can easily calculate the Mn valency (ν) according to the chemical formulas $CaMn^{4+}_{1-2x}Mn^{3+}_xRu^{5+}_xO_3$ $[\nu=(4-5x)/(1-x)]$, $CaMn^{4+}_{1-3y}Mn^{3+}_{2y}Mo^{6+}_yO_3$ $[\nu=(4-6y)/(1-y)]$, and $Ca_{1-x}Sm_xMn^{4+}_{1-x}Mn^{3+}_xO_3$ $(\nu=4-x)$.

The ν dependence of the lattice parameters and volume is similar for the three series, as illustrated Fig. 1, suggesting the reasonableness of the assumption that Ru is pentavalent, in agreement with previous observations.[18,20,22] Thermopower measurements had indeed been used to estimate the Ru valency.[18] The room-temperature value of S directly depends on the carrier concentration[15] and gives therefore an estimate of the doping cation valency. TEP measurements had been performed in the system $CaMn_{0.94}M_{0.06}O_3$ with M = Nb, Re, Sn, and Ru. For Nb^{5+} and Re^{5+}, S was ranging from -80 to -120 μV/K at 300 K while S was close to -320 μV/K for Sn^{4+}. As S is equal to -140 μV/K at 300 K for $CaMn_{0.94}Ru_{0.06}O_3$, the valency of Ru was estimated to be close to Ru^{5+}.

Figure 1 also shows clearly that, in this valency range, the perovskite cell remains O type, which is $a>b/\sqrt{2}>c$, i.e., without the cooperative Jahn-Teller effect.

Resistivity and magnetic behaviors

Although the substitutions of Ru^{5+} or Mo^{6+} at the Mn site are both responsible for a valency change of Mn, the transport and magnetic properties are found to exhibit different features. Figure 2 gives the temperature dependence of resistivity of $CaMn_{1-x}Ru_xO_3$ ($x=0.04$, 0.06, and 0.08). All samples exhibit insulating behavior at the lowest temperature. Under an applied magnetic field up to 7 T, the resistivity at low temperature shows a large negative magnetoresistance. The resistivity ratio defined as $\rho(0)/\rho(H=7\text{ T})$ reaches 12 at 5 K for the $x=0.06$ sample. At the same time, the doping with ruthenium induces an obvious decrease in resistivity. The resistivity at 5 K of the $x=0.08$ sample is 1.6×10^3 Ω cm, two orders smaller than that of $x=0.04$ sample, 4.5×10^5 Ω cm. From previous works[15,18] we know that the transport mechanism at high temperature can be described by small polaron hopping model. So we used $\rho=AT\exp(W/k_BT)$ to fit the high-temperature region (150–300 K) of the resistivity at zero field. The fitting parameters are listed in Table I, which shows that activation energy W decreases from 45.4 meV ($x=0.04$) to 36.2 meV ($x=0.08$), confirming the more conductive character induced by the Ru doping. From the fitting results shown in Fig. 2(b), it can be seen that at low temperature the fitting curves do not agree with the experimental data, indicating some transitions with cooling. Magnetization (M) measurements demonstrate this point of view.

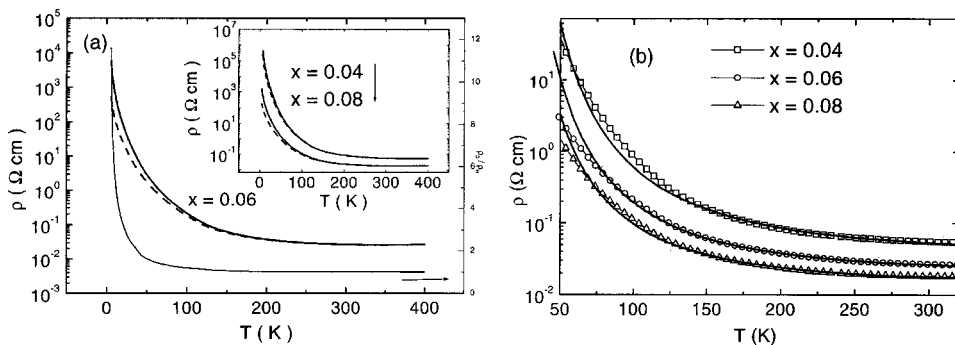Figure 3(a) shows the M-T curves of all Ru-doped samples. At about 125 K, which is just the antiferromagnetic

FIG. 2. (a) $\rho-T$ curves of $CaMn_{1-x}Ru_xO_3$. The solid lines and the dashed lines represent the curves at zero field and 7 T magnetic field, respectively. The resistivity ratio $\rho_0/\rho_{7T}(T)$ of $x=0.06$ is also given (right y-axis). (b) Small polaron model fitting results, the open symbols are for experimental data and the solid lines for fitting curves.

TABLE I. Fitting parameters of the transport and magnetic curves.

Composition		A (Ω cm)	W (meV)	Θ (K)
CaMnO$_3$		2.69×10^{-4}	5.4	
CaMn$_{1-x}$Ru$_x$O$_3$	$x=0.04$	3.07×10^{-5}	45.4	-165
	$x=0.06$	2.00×10^{-5}	40.0	-28
	$x=0.08$	1.46×10^{-5}	36.2	39
CaMn$_{1-y}$Mo$_y$O$_3$	$y=0.02$	2.56×10^{-5}	6.18	-13
	$y=0.04$	1.45×10^{-5}	10.5	53

(AFM) transition temperature of CaMnO$_3$, the magnetization rises and keeps increasing with cooling. The zero-field-cooling (ZFC) curves and field-cooling (FC) curves also disperse at that temperature, which suggests that there is a complex magnetic structure in the samples. With the increase of ruthenium content, the magnetization is enhanced although still small. We replotted the zero-field cooling curves as $1/M \sim T$ relations [Fig. 3(b)]. Above the transition temperature the curves can be linearly fitted very well. The fitting parameters listed in Table I show that the Curie-Weiss temperature Θ in the relation $\chi = C/(T-\Theta)$ changes from -165 K ($x=0.04$) to 39 K ($x=0.08$), which means that the magnetic interactions change from antiferromagnetic to ferromagnetic with doping. All these results indicate that ruthenium induces ferromagnetism in the antiferromagnetic matrix of the samples.

For the Mo-doped samples CaMn$_{1-y}$Mo$_y$O$_3$ ($y=0.02$ and 0.04), the situation is somewhat different. The resistivity (shown in Fig. 4) goes through a broad minimum around 170 K for $y=0.02$ and 200 K for $y=0.04$ and increases again with cooling at lower temperature, while for Ru doping this minimum is expected to take place at higher temperatures. The value of resistivity is much smaller than that of Ru-doped samples. Under an applied magnetic field, the resistivity of the samples is also strongly reduced, the CMR ratio reaches 12 at low temperature for $y=0.04$. With the increase of molybdenum content, the resistivity decreases and exhibits a shoulder on the ρ-T curve at about 100 K [$y=0.04$, Fig. 4(a)]. The fitting, which is done according to the small polaron hopping model, shows that despite the fact that the resistivity decreases, the activation energy W increases with doping (Table I), which is opposite to the Ru-doping case. The magnetization measurements demonstrate that the in-

flection of ρ-T curve for $y=0.04$ at about 100 K is caused by a magnetic transition. In Fig. 5(a), the M-T zero-field-cooling curve of $y=0.02$ sample shows a peak at 75 K. The difference between the zero-field-cooling curve and field-cooling curve is small compared to the other compound. The fitting of the $1/M$-T curve [Fig. 5(b)] shows that antiferromagnetic fluctuations dominate the paramagnetic regime ($\Theta = -13$ K). As the doping content increases to 4%, the transition temperature shifts to about 90 K, just near the inflection temperature of ρ-T curve. The difference between the ZFC and FC curves becomes obvious. The magnetization increases and the fitting parameter Θ is positive (53 K). All these indicate that below the transition temperature there are some ferromagnetic clusters existing in the system. As a result, the itinerancy of the electrons is reinforced below that temperature, but the content of FM clusters does not reach the percolation threshold. Therefore only a shoulder appears on the ρ-T curve.

Comparison between CaMn$_{1-x}$Ru$_x$O$_3$ and CaMn$_{1-y}$Mo$_y$O$_3$

The emergence of ferromagnetism in the samples can be explained by the fact that the high-valency dopants can induce Mn^{3+} species in the samples. As a consequence, the double exchange between Mn^{3+} and Mn^{4+} can be established. So at a certain temperature, many ferromagnetic clusters come into being in the system. With the increase in doping content, the number of FM clusters increases, which enhances the magnetization. However, compared to the ruthenium-doping case, the magnetization of Mo-doped samples is much larger (Table II). For instance, CaMn$_{0.98}$Mo$_{0.02}$O$_3$ and CaMn$_{0.96}$Ru$_{0.04}$O$_3$, which both exhibit a very similar Mn valency, $\nu_{Mn} \approx 3.96$, show very different M values. The maximum M value under a 100 Oe magnetic field from the zero-field-cooling curve for the Ru-doped sample is $1.5\times10^{-4}\mu_B$, while that of the Mo-doped sample is $3.1\times10^{-2}\mu_B$. This suggests an antiferromagnetic behavior for CaMn$_{1-x}$Ru$_x$O$_3$ with $x \leqslant 0.06$, contrasting with the FM properties observed for CaMn$_{1-y}$Mo$_y$O$_3$ and also for other CaMn$_{1-x}$M$_x$O$_3$ series with $M=$ Nb, Ta, and W.[17] In order to check the magnetic state induced by Ru, neutron powder-diffraction experiments have been performed for CaMn$_{0.94}$Ru$_{0.06}$O$_3$. The temperature dependence of the patterns shows that no structural transition occurs from 1.5 to 300 K (Fig. 6). The cell lattice remains *Pnma* with small orthorhombic distortion $D=0.137$ and 0.198 at 1.5 and 300 K, respectively (calculated from the $D=\frac{1}{3}\Sigma(a_i - \langle a \rangle)/\langle a \rangle$
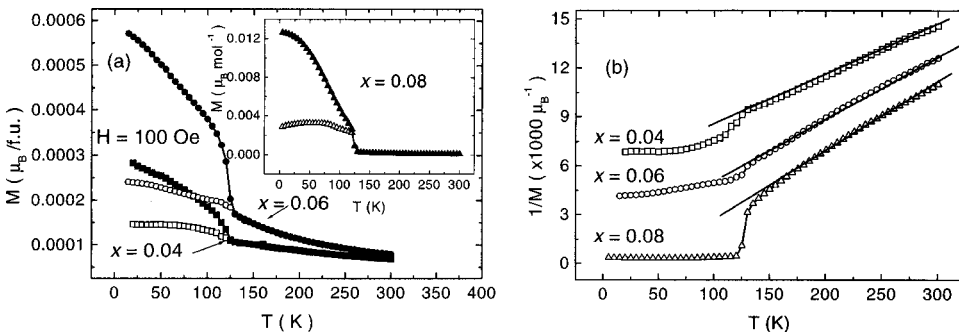

FIG. 3. (a) The temperature dependence of magnetization of CaMn$_{1-x}$Ru$_x$O$_3$. The open symbols represent zero-field-cooling-curves, the solid ones represent field cooling curves. (b) $1/M-T$ curves. The high-temperature region can be linearly fitted well. All data were registered under 100 Oe magnetic field.
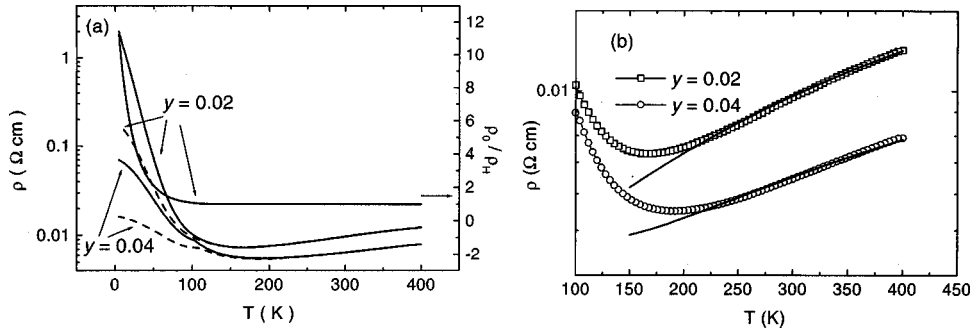
FIG. 4. (a) $\rho-T$ curves of $CaMn_{1-y}Mo_yO_3$. The solid lines and the dashed lines represent the curves at zero field and 7 T magnetic field, respectively. The right y-axis curves correspond to the resistivity ratio $\rho_0/\rho_{7T}(T)$ of $y=0.02$. (b) Small polaron model fitting results, the open symbols are for experimental data and the solid lines for fitting curves.
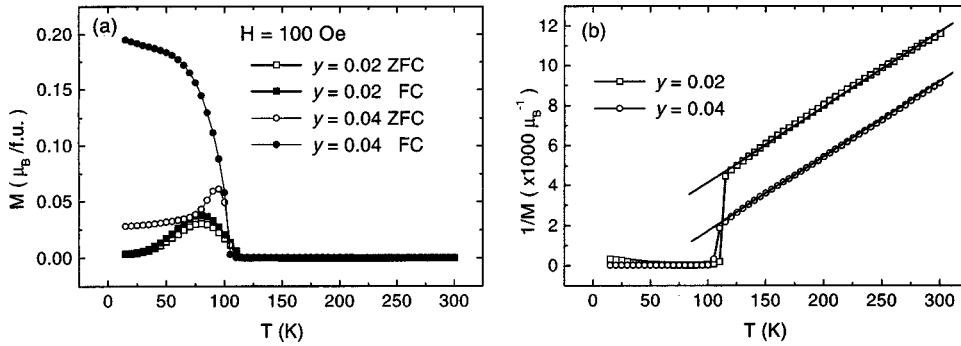

FIG. 5. (a) $M-T$ curves of $CaMn_{1-y}Mo_yO_3$. The open symbols represent zero field cooling curves, the solid ones represent field cooling curves. (b) $1/M-T$ curves. All data were registered under 100 Oe magnetic field.

TABLE II. Comparison of magnetization and resistivity values between $CaMn_{1-x}Ru_xO_3$ and $CaMn_{1-y}Mo_yO_3$ with the same Mn valency. The magnetization values are obtained from zero-field-cooling curves measured under a 100 Oe magnetic field.

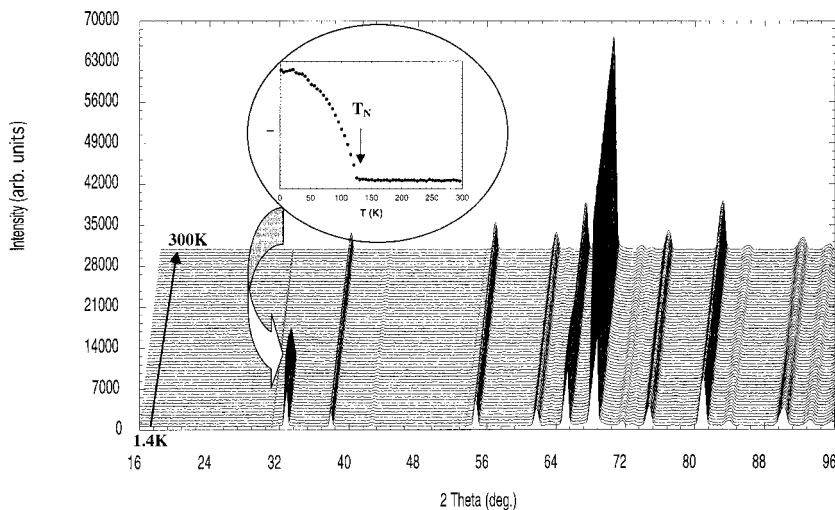| ν_{Mn}	Doping content	$M_{max}(\mu_B)$	ρ (5 K) (Ω cm)	ρ (300 K) (Ω cm)
~3.96	Ru, 0.04	1.5×10^{-4}	5.0×10^5	5.6×10^{-2}
	Mo, 0.02	3.1×10^{-2}	2.0	9.7×10^{-3}
~3.92	Ru, 0.08	3.2×10^{-3}	1.6×10^3	1.9×10^{-2}
	Mo, 0.04	6.1×10^{-2}	7.0×10^{-2}	6.5×10^{-3}

FIG. 6. $CaMn_{0.94}Ru_{0.06}O_3$ neutron powder diffraction patterns ($\lambda=2.4266$ Å), recorded from 1.4 to 300 K. The intensity of the 110 peak, characteristic of the G-type AFM state, versus T is also given in inset.

$\times 100$ formula). Nevertheless, a clear magnetic transition is evidenced around 125 K (inset of Fig. 6). Below this T_N ≈ 125 K, CaMn$_{0.94}$Ru$_{0.06}$O$_3$ exhibits a G-type AFM state, the magnetic moment is refined to 2.33(2)μ_B at 1.4 K (i.e., 78% of the theoretical expected value). No FM component has been detected contrary to the case of Sm$_{0.1}$Ca$_{0.9}$MnO$_3$,[23] in agreement with the lower magnetization values registered for the Ru series than the Sm one. Thus, the magnetic character of Ru^{5+} ($4d^3$; t_{2g}^3; $S = \frac{1}{2}$) must be considered to interpret this result. The antiferromagnetic coupling between e_g^0 cations, Ru^{5+} and Mn^{4+} dominates clearly for lower doping contents. This interaction prevails over positive Mn^{3+}-O-Mn^{4+} and Ru^{5+}(e_g^0)-O-Mn^{3+}(e_g^1) magnetic exchange. On the other hand, for molybdenum doping (Mo^{6+}; d^0), this non-magnetic dopant does not couple with Mn^{3+} and Mn^{4+} ions. It just indirectly induces ferromagnetism via the Mn^{3+} creation at the expense of the Mn^{4+}-O-Mn^{4+} antiferromagnetic interaction. The effect of Mo doping is thus very similar in this respect to the A-site doping in the Ca$_{1-x}$Sm$_x$MnO$_3$ system.[14] This emphasizes the peculiar role of Ru: the dominating AFM interaction between Ru^{5+}-O-Mn^{4+} explains why the ferromagnetism in Ru-doped system is much weaker than that in the Mo-doped system for small concentrations. But for larger Ru content, FM properties are found to be in agreement with increasing numbers of Mn^{3+} in the matrix that favor the FM Ru^{5+}-O-Mn^{3+} interaction.

For the same doping level, the amount of the ferromagnetic phase inside the samples is larger in the case of Mo than that for M = Ru, and the resistivity of the materials tends to decrease because the dopants also increase the number of Mn^{3+} carriers in the Mn^{4+} matrix, and the DE interaction reinforces the itinerancy of these carriers below T_C. So by increasing the doping content, the conductivity is globally increased. Introducing Mn^{3+} carriers in CaMnO$_3$ by A-site doping had also the same influence.[14] But for M = Ru, the conductivity, especially at low temperature, is far smaller than that for M = Mo (Table II). For the same Mn mixed valency induced by small amounts of impurity, the resistivity at 5 K for Ru-doped samples is several orders larger than that for Mo-doped samples [which exhibit resistivity values close to Ca$_{1-x}$Sm$_x$MnO$_3$ with $x \leqslant 0.1$ (Ref. 14)]. Obviously the antiferromagnetic coupling between Ru^{5+} and Mn^{4+} at low temperature in Ru-doped samples is responsible for this big difference. Nevertheless, for higher Ru content the conductivity starts to increase as a result of the Ru^{5+}-O-Mn^{3+} FM interactions.[20,24]

On the other hand, the Mn^{3+} ions induced by the dopants enhance the Jahn-Teller distortion in the materials and make the system tend to form small polarons. The dopants play the role of scattering centers inside the Mn network. Therefore, the activation energy should increase as the doping content gets larger. For the Mo-doping situation, the fitting results confirm that point. As for Ca$_{1-x}$Sm$_x$MnO$_3$,[25] the activation energy increases with doping. But for Ru-doped samples, the activation energy decreases with increasing doping content. We believe it is due to the e_g^0 states of ruthenium that can participate in band formation by coupling with Mn^{3+} (e_g^1) and contribute to make it broader.[24] After the doping content
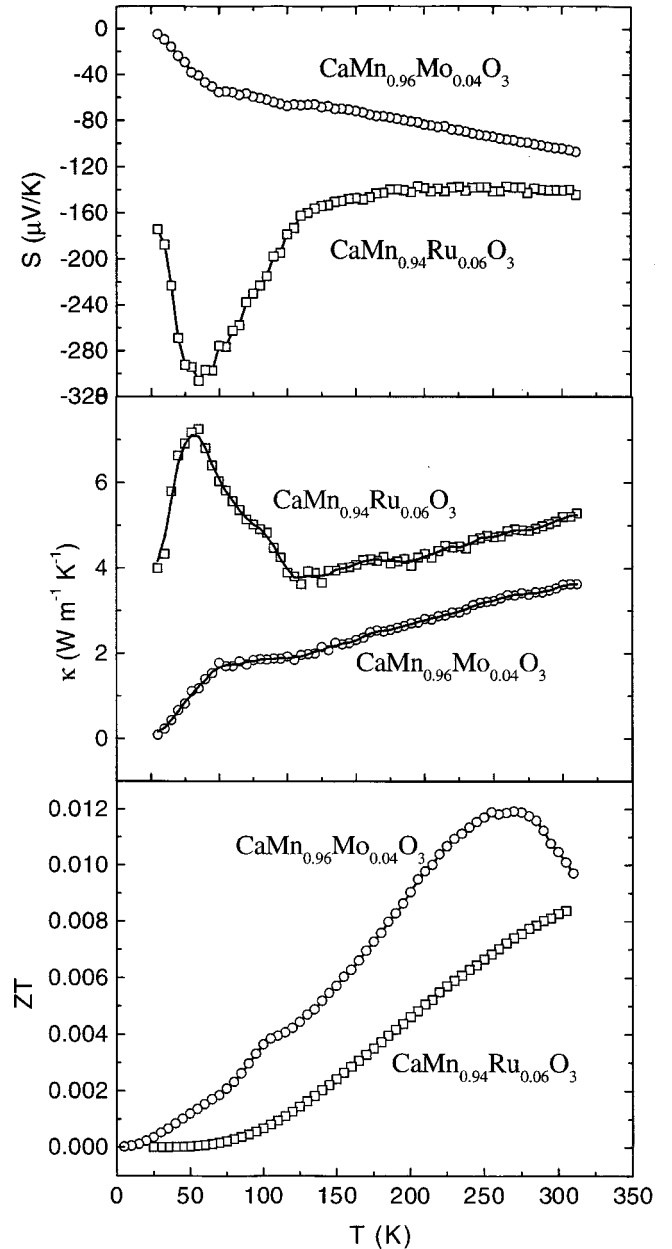

FIG. 7. The temperature dependence of thermopower, thermal conductivity, and factor ZT of CaMn$_{0.94}$Ru$_{0.06}$O$_3$ and CaMn$_{0.96}$Mo$_{0.04}$O$_3$.

reaches a certain percentage, this effect would become dominant, which decreases the activation energy rather than increases it.

Thermopower

These different magnetic behaviors for low doping of Ru and Mo are also reflected in the thermopower measurement results. The S-T curves (shown in Fig. 7) have a change of slope at 120 K for CaMn$_{0.94}$Ru$_{0.06}$O$_3$ and 110 K for CaMn$_{0.96}$Mo$_{0.04}$O$_3$, which are just their magnetic transition temperatures, respectively. If we plot the $d[\ln(\rho/T)]/d(1/T)$-T curve, inflections can be seen at those temperatures. This indicates that the electronic transport

mechanism has changed because of the magnetic transition, which also alters the behaviors of the temperature dependence of thermopower. The interesting point is that the absolute value of the thermopower at room temperature of these electron-doped materials is rather large, together with low thermal conductivity. For $CaMn_{0.94}Ru_{0.06}O_3$, S at 300 K is about -140 $\mu V K^{-1}$ and $\kappa \approx 5 W K^{-1} m^{-1}$. For $CaMn_{0.96}Mo_{0.04}O_3$, S also reaches about -110 $\mu V K^{-1}$ with $\kappa \approx 3.5 W K^{-1} m^{-1}$. It is well known that S is sensitive at high temperature to the carrier concentration and follows the fomula

$$S = -\frac{\pi^2 k_B^2}{3e} T \left(\frac{N(E)}{n} + \text{const} \right)_{E=E_F},$$

in which $N(E)$ is the density of states and n is the carrier density.[15] The smaller the n, the larger the $|S|$. Although the doping content of the foreign cation in $CaMn_{0.96}Mo_{0.04}O_3$ is smaller than that in $CaMn_{0.94}Ru_{0.06}O_3$, the carrier concentration in $CaMn_{0.96}Mo_{0.04}O_3$ is larger because the Mo valency is $+6$ while that of Ru is $+5$.[20,22] Therefore the Ru-doped sample has a larger $|S|$ value at 300 K. The large negative thermopower of these materials makes them valuable to be n-type legs for a thermoelectric device as previously reported for $Ca_{1-x}La_xMnO_3$ manganite.[16] In order to make a comparison of their ability for application, we calculated their figure of merit, $Z = S^2/\rho\kappa$ (Fig. 7), where $\rho(T)$ is from Figs. 2 and 4 and $S(T)$ and $\kappa(T)$ are from Fig. 7. It is known that the material that is suitable for application should have large S, small κ, and small resistivity and be characterized by a large figure of merit. As can be seen, the ZT value of the Mo-doped sample starts to decrease with increasing temperature ($T > 250$ K), which is unsuitable for the application at high temperature. In contrast, for the Ru-doped sample, the ZT value is still increasing with temperature. Therefore, although its ZT value at 300 K is rather small [about 0.01 but not far from the value of $NaCo_2O_4$, 0.032 (Ref. 26)], we can estimate that it would have a larger ZT value at higher tem-perature. Furthermore, as in the case of $NaCo_2O_4$, a large reduction of ρ is expected in the case of single crystals, which could strongly improve Z.

CONCLUSION

In summary, we have synthesized two sets of samples, $CaMn_{1-x}Ru_xO_3$ and $CaMn_{1-y}Mo_yO_3$. In the low doping range for both sets, the doping decreases the resistivity and increases the magnetization, which indicates the creation of ferromagnetic clusters with doping. This is consistent with the pentavalent and hexavalent oxidation states for ruthenium and molybdenum, respectively. Nevertheless, for low dopant concentration, at the same doping level, Mo-doped samples have much smaller resistivity and larger magnetization. This can be explained by two features. First, Mo has a higher valency than Ru and creates a larger concentration of Mn^{3+}, favoring a Mn^{3+}/Mn^{4+} double-exchange interaction. Second, the antiferromagnetic state revealed by neutron powder diffraction competes with FM interactions for low doping levels in the case of Ru as exemplified for $CaMn_{0.94}Ru_{0.06}O_3$, due to an AFM coupling between Ru^{5+} and Mn^{4+} ions. Another difference is that Mo doping increases the activation energy while Ru doping decreases it. This can be understood by the fact that for Ru-doped samples, the e_g^0 states of ruthenium can contribute to the broadening of the band due to the Ru^{5+}-O-$Mn^{3+} \Leftrightarrow Ru^{4+}$-O-$Mn^{4+}$ equilibrium. With large thermopower, low thermal conductivity, and small resistivity, these materials are good candidates for applications as n-type legs of thermopower generators to be used at high temperatures ($T \gg 300$ K).

ACKNOWLEDGMENTS

*Corresponding author. Email address: antoine.maignan@ismra.fr

[1] R. Von Helmolt, J. Wecker, B. Holzapfel, L. Schultz, and K. Samwer, Phys. Rev. Lett. **71**, 2331 (1993).

[2] C. Zener, Phys. Rev. **82**, 403 (1951).

[3] A. J. Millis, P. B. Littlewood, and B. I. Shraiman, Phys. Rev. Lett. **74**, 5144 (1995).

[4] S. Jin, T. H. Tiefel, M. McCormack, R. A. Fastnact, R. Ramesh, and L. H. Chen, Science **264**, 413 (1994).

[5] H. L. Ju, C. Kwon, Q. Li, R. L. Greence, and T. Vankatesan, Appl. Phys. Lett. **65**, 2108 (1994).

[6] S. S. Manoharan, N. Y. Vasanthachaya, M. S. Hegde, K. M. Satyalakshmi, V. Prasad, and S. V. Subramanyam, J. Appl. Phys. **76**, 3923 (1994).

[7] G. C. Xiong, Q. Li, H. L. Ju, R. L. Greence, and T. Venkatesan, Appl. Phys. Lett. **66**, 1689 (1995).

[8] S. K. Singh, S. B. Palmer, D. Mck. Paul, and M. R. Lees, Appl. Phys. Lett. **69**, 263 (1996).

[9] W. Bao, J. D. Axe, C. H. Chen, and S. W. Cheong, Phys. Rev. Lett. **78**, 543 (1997).

[10] Y. Murakami, D. Shindo, H. Chiba, M. Kikuchi, and Y. Syono, Phys. Rev. B **55**, 15 043 (1997).

[11] E. O. Wollan and W. C. Koehler, Phys. Rev. **100**, 545 (1955).

[12] H. Chiba, M. Kikuchi, K. Kusaba, and Y. Syono, Solid State Commun. **99**, 499 (1996).

[13] I. O. Troyanchuk, N. V. Samsonenko, H. Szymczak, and A. Nabialek, J. Solid State Chem. **131**, 144 (1997).

[14] C. Martin, A. Maignan, F. Damay, M. Hervieu, and B. Raveau, J. Solid State Chem. **134**, 198 (1997).

[15] J. Hejtmánek, Z. Jirák, M. Maryško, C. Martin, A. Maignan, M. Hervieu, and B. Raveau, Phys. Rev. B **60**, 14 057 (1999).

[16] I. Matsubara, R. Funahashi, T. Takeuchi, S. Sodeoka, T. Shimizu, and K. Ueno, Appl. Phys. Lett. **78**, 3627 (2001).

[17] B. Raveau, Y. M. Zhao, C. Martin, M. Hervieu, and A. Maignan, J. Solid State Chem. **149**, 203 (2000).

[18] B. Raveau, A. Maignan, C. Martin, and M. Hervieu, Mater. Res. Bull. **35**, 1579 (2000).

[19] C. Martin, A. Maignan, M. Hervieu, B. Raveau, and J. Hejt-

COMPARISON OF CaMn$_{1-x}$Ru$_x$O$_3$ AND CaMn$_{1-y}$Mo$_y$O$_3$ ...

PHYSICAL REVIEW B **67**, 024430 (2003)

manek, Phys. Rev. B **63**, 100406 (2001).

[20] A. Maignan, C. Martin, M. Hervieu, and B. Raveau, Solid State Commun. **117**, 377 (2001).

[21] A. Maignan, C. Martin, C. Autret, M. Hervieu, B. Raveau, and J. Hejtmanek, J. Mater. Chem. **12**, 1806 (2002).

[22] P. D. Battle and C. W. Jones, J. Solid State Chem. **78**, 108 (1989); P. D. Battle, T. C. Gibb, C. W. Jones, and F. Studer, J. Solid State Chem. **78**, 281 (1989); P. D. Battle, C. W. Jones, and F. Studer, J. Solid State Chem. **90**, 302 (1991).

[23] C. Martin, A. Maignan, M. Hervieu, B. Raveau, Z. Jirák, M. M. Savosta, A. Kurbakov, V. Trounov, G. André, and F. Bourée, Phys. Rev. B **62**, 6442 (2000).

[24] C. Martin, A. Maignan, M. Hervieu, C. Autret, B. Raveau, and D. I. Khomskii, Phys. Rev. B **63**, 174402 (2001).

[25] A. Maignan, C. Martin, F. Damay, B. Raveau, and J. Hejtmanek, Phys. Rev. B **58**, 2758 (1998).

[26] I. Terasaki, in *Proceedings of the 18th International Conference on Thermoelectrics (ICT'99), Baltimore, 1999* (IEEE, Piscataway 2000), p. 569.